AFCRL-71-0371
30 APRIL 1971
ENVIRONMENTAL RESEARCH PAPERS, NO. 360

AIR FORCE CAMBRIDGE RESEARCH LABORATORIES
L. G. HANSCOM FIELD, BEDFORD, MASSACHUSETTS

Scattering of HF Radio Waves by a Spherical Electron Cloud in the Presence of a Magnetic Field

MILTON M. KLEIN
NORMAN W. ROSENBERG

AIR FORCE SYSTEMS COMMAND
United States Air Force

Unclassified
Security Classification

DOCUMENT CONTROL DATA - R&D

(Security classification of title, body of abstract and indexing annotation must be entered when the overall report is classified)

1. ORIGINATING ACTIVITY *(Corporate author)*
Air Force Cambridge Research Laboratories (LKC)
L. G. Hanscom Field
Bedford, Massachusetts 01730

2a. REPORT SECURITY CLASSIFICATION
Unclassified

2b. GROUP

3. REPORT TITLE
SCATTERING OF HF RADIO WAVES BY A SPHERICAL ELECTRON CLOUD IN THE PRESENCE OF A MAGNETIC FIELD

4. DESCRIPTIVE NOTES *(Type of report and inclusive dates)*
Scientific. Interim.

5. AUTHOR(S) *(First name, middle initial, last name)*
Milton M. Klein
Norman W. Rosenberg

6. REPORT DATE	7a. TOTAL NO. OF PAGES	7b. NO. OF REFS
30 April 1971	33	8

8a. CONTRACT OR GRANT NO.		9a. ORIGINATOR'S REPORT NUMBER(S)
b. PROJECT, TASK, WORK UNIT NOS.	7635-13-01	AFCRL-71-0371
c. DOD ELEMENT	62101F	9b. OTHER REPORT NO(S) *(Any other numbers that may be assigned this report)*
d. DOD SUBELEMENT	681000	ERP No. 360

10. DISTRIBUTION STATEMENT
1-This document has been approved for public release and sale; its distribution is unlimited.

11. SUPPLEMENTARY NOTES	12. SPONSORING MILITARY ACTIVITY
TECH, OTHER	Air Force Cambridge Research Laboratories (LKC) L.G. Hanscom Field Bedford, Massachusetts 01730

13. ABSTRACT

The scattering of HF radio waves by a spherical electron cloud in the presence of a magnetic field has been obtained in ray optics approximation for a Gaussian distribution of electron density. The effect of a magnetic field is small at 30 MHz, but substantial at 3 MHz. The scattering in the forward direction is independent of critical radius and magnetic field. The displacement of the backscattered ray from the axis of symmetry of the cloud shows a strong dependence upon field angle with maximum effects at ±45°. The cross section for the ordinary ray is strongly dependent on field angle with a maximum near 90°, the effect decreasing as the critical radius increases. The extraordinary ray shows a minimum cross section near 90°, with much less dependence on field angle. The maximum scattering angle for underdense spheres exhibits a moderate dependence upon field angle for the ordinary ray, and virtually none for the extraordinary. It is shown that the backscatter data for the extraordinary ray may be analyzed in terms of an effective critical radius which depends upon the gyromagnetic ratio, with a small correction for the effect of field angle.

The objective of this report is to provide knowledge and understanding of the effect of the earth's magnetic field upon the propagation of electromagnetic waves through the ionosphere, ionospheric irregularities, and artificial electron clouds. It is thus directed to the furnishing of data, together with criteria, for the solution of Air Force problems of discrimination, detection, and communication.

DD FORM 1 NOV 68 1473

Unclassified
Security Classification

14. KEY WORDS	LINK A		LINK B		LINK C	
	ROLE	WT	ROLE	WT	ROLE	WT
Scattering						
Magnetic field						
Radio waves						
Plasma cloud						
Ray optics						

AFCRL-71-0371
30 APRIL 1971
ENVIRONMENTAL RESEARCH PAPERS, NO. 360

AERONOMY LABORATORY PROJECT 7635
AIR FORCE CAMBRIDGE RESEARCH LABORATORIES
L. G. HANSCOM FIELD, BEDFORD, MASSACHUSETTS

Scattering of HF Radio Waves by a Spherical Electron Cloud in the Presence of a Magnetic Field

MILTON M. KLEIN
NORMAN W. ROSENBERG

AIR FORCE SYSTEMS COMMAND
United States Air Force

Abstract

The scattering of HF radio waves by a spherical electron cloud in the presence of a magnetic field has been obtained in ray optics approximation for a Gaussian distribution of electron density. The effect of a magnetic field is small at 30 MHz, but substantial at 3 MHz. The scattering in the forward direction is independent of critical radius and magnetic field. The displacement of the backscattered ray from the axis of symmetry of the cloud shows a strong dependence upon field angle with maximum effects at ±45°. The cross section for the ordinary ray is strongly dependent on field angle with a maximum near 90°, the effect decreasing as the critical radius increases. The extraordinary ray shows a minimum cross section near 90°, with much less dependence on field angle. The maximum scattering angle for underdense spheres exhibits a moderate dependence upon field angle for the ordinary ray, and virtually none for the extraordinary. It is shown that the backscatter data for the extraordinary ray may be analyzed in terms of an effective critical radius which depends upon the gyromagnetic ratio, with a small correction for the effect of field angle.

The objective of this report is to provide knowledge and understanding of the effect of the earth's magnetic field upon the propagation of electromagnetic waves through the ionosphere, ionospheric irregularities, and artificial electron clouds. It is thus directed to the furnishing of data, together with criteria, for the solution of Air Force problems of discrimination, detection, and communication.

Contents

Illustrations

Illustrations

Scattering of HF Radio Waves by a Spherical Electron Cloud in the Presence of a Magnetic Field

1. INTRODUCTION

During the past several years, the Air Force Cambridge Research Laboratories have been engaged in studies of the upper atmosphere through the release of artificial ionized clouds. A part of this study involves the use of radar to obtain the electron density distribution and its maximum value within the cloud. To aid in the interpretation and correlation of data, a systematic study is being conducted on the scattering of high-frequency radio waves by electron clouds. Since the cloud size is large in comparison to the wavelength, the investigation is being made within the framework of geometrical optics.

For the case of zero magnetic field, the scattering amplitude may be obtained as a function of scattering angle by evaluation of the scattering integral (Bohm, 1951). This procedure has been utilized in order to obtain the scattering from a spherical electron cloud with a Gaussian distribution of electron density in the radial direction (Klein and Mabee, 1969). When the effect of the magnetic field is taken into account, the index of refraction becomes a function of ray direction as well as of position. As a consequence, the scattering amplitude cannot be obtained directly. Instead, the ray paths must first be computed by a suitable technique and the scattering then obtained from the angular displacement of neighboring rays as a function of impact parameter.

(Received for publication 30 April 1971)

To obtain the ray paths, we have utilized the method developed by Haselgrove (1955), which expresses the ray propagation in terms of a set of first-order differential equations in space and time. The form of these equations is particularly amenable to solution by high-speed digital computers. As an initial phase of the investigation, it is assumed that the cloud is spherical, with a spherically symmetric electron density distribution, and that the effect of absorption is negligible. As indicated by diffusion theory, the electron density is considered to have a Gaussian distribution in the radial direction.

Initial calculations by the Haselgrove procedure were presented at the Fourteenth Symposium of the Electromagnetic Wave Propagation Committee of AGARD in Norway (Rosenberg et al, 1968). At that time difficulties were encountered with the determination of the path for the ordinary ray at small input parameters where the ray reaches the critical surface and a cusp or "spitze" phenomenon occurs (Poeverlein, 1950). The scattering amplitude for the ordinary ray exhibited very low values in the backscatter region. Inasmuch as these results did not appear trustworthy, they were left incomplete. However, since that time the computer program has been improved to the effect that the ordinary ray can be calculated accurately in the region of small impact parameters; the cross section no longer exhibits very low values in the backscatter region.

2. ANALYSIS

A ray initially a distance b from the x axis, or axis of propagation, is deflected through an angle θ as it emerges from the cloud (Figure 1). The Haselgrove equations for the ray paths are

$$\frac{dx}{dt} = \frac{c}{\mu^2}\left(\mu \cos\alpha + \frac{\partial\mu}{\partial\alpha}\sin\alpha\right). \tag{1}$$

$$\frac{dz}{dt} = \frac{c}{\mu^2}\left(\mu \sin\alpha - \frac{\partial\mu}{\partial\alpha}\cos\alpha\right). \tag{2}$$

$$\frac{d\alpha}{dt} = \frac{c}{\mu^2}\left(\frac{\partial\mu}{\partial x}\sin\alpha - \frac{\partial\mu}{\partial z}\cos\alpha\right). \tag{3}$$

Here μ is the index of refraction, c the velocity of light, and α the angle the wave normal makes with the direction of propagation. Since the constant factor c has no effect upon the geometry of the ray, it may be absorbed conveniently in the time factor t. The index of refraction is given by the Appleton-Hartree equation, which for the case of no absorption has the form (Kelso, 1964a)

$$\mu^2 = 1 - \frac{2X(1-X)}{2(1-X) - Y_T^2 \pm [Y_T^4 + 4Y_L^2 (1-X)^2]^{1/2}} , \qquad (4)$$

where $X = \frac{\omega_n^2}{\omega^2}$, ω_n and ω are the plasma and incident frequencies, Y_T and Y_L are the transverse and longitudinal components of the gyromagnetic ratio Y, and θ_p is the angle between the direction of propagation and the earth's magnetic field H_e. The (+) sign refers to the ordinary ray and the (-) sign to the extraordinary ray. Because of the form of Eq. (4), the scattering phenomena will have a period of 180° with results at $-\theta_p$ the same as those at 180° - θ_p.

If the incident rays are confined to the magnetic meridian plane, that is, the plane containing the direction of propagation and the magnetic field direction, then no lateral deviations occur (Budden, 1966). However, for rays outside of this plane, lateral deviations do occur, but numerical solutions indicate these to be small (Kelso, 1964b). The effect of lateral deviations will not be considered here.

For a Gaussian distribution, the electron density n has the form

$$n = n_o \exp(-r^2/a^2) , \qquad (5)$$

where n_o is the center point density and a the Gaussian radius. If we define a parameter r_c by

$$r_c|r_c| = \ln\left(\frac{n_c}{n_o}\right) , \qquad (6)$$

where n_c is the critical plasma density for the ordinary ray (X = 1), the electron density may then be written as

$$\frac{n}{n_c} = \exp\left[(r_c|r_c| - r^2)/a^2\right] , \qquad (7)$$

a plot of which is shown in Figure 2. We note that for overdense plasmas, n_c occurs at a radius equal to r_c, that is, r_c is the critical radius at which the local density is critical. For plasmas underdense at the center, r_c is negative but significant refraction still may occur. For convenience, we shall use the descriptive term critical radius for both positive and negative r_c. Referring to Figure 3, which gives ray diagrams for both overdense and underdense spheres, we note that a series of rays coming from the left are refracted by different amounts depending

on the impact parameter b, the initial z distance above the axis of symmetry. For large values of b there is little or no refraction. For a ray at small b, bending occurs to a final angle ranging from 0° through 90° to 180° as the impact parameter decreases to zero, or from the lower side from 0° to -90° to -180°, as the impact parameter increases to zero. Note that the direction -180° is identical to +180°, both indicating complete backscatter.

In an underdense plasma, the refraction increases from 0° to some maximum angle, say 90°, returning to 0 as the impact parameter reaches zero. Thus, complete backscatter never occurs and therefore all energy is scattered in the forward direction.

From the solution of the Haselgrove equations, which yield the increment in scattering angle $\Delta\theta$ corresponding to an increment Δb in the impact parameter, the cross section $\sigma(\theta)$ is calculated from

$$\sigma(\theta) = \frac{4\pi\, b\Delta b}{\sin\theta\, \Delta\theta} \tag{8}$$

The scattering angle and the cross section may then be presented as a function of critical radius, frequency, magnetic field direction, and polarization (ordinary or extraordinary ray).

3. METHOD OF CALCULATION

The computer solution of the ray tracing problem is based on the Haselgrove set of differential equations, which fixes ray and phase angle from local density and density derivatives. With the assumed Gaussian distribution, ordinary and extraordinary rays were traced for a matrix of two frequencies, four magnetic field angles, and seven values of critical radius, with a fixed Gaussian radius of 1 kilometer. The earth's magnetic field H_e was taken as 0.36 gauss.

Rays were launched in the x direction from a surface 8 km from the center of the plasma, at a series of 21 z distances (impact parameters) above and below the center (Figure 3), ranging from -4 to +4 km; each ray trace ended when the ray passed out through the 8-km surface, noting the final ray angle with respect to the incident ray direction. Steps in each ray trace were limited to a maximum time increment chosen to limit the change in refractive index to less than 20 percent and further, to limit the change in ray angle to less than a fixed increment $d\theta$ (1°, 0.5°, 0.25°, and so on).

At each step, a Runge-Kutta approximation to the Haselgrove equations was made to determine increments in x, z, and phase angle, which were then used to determine the effective refractive index at the new x,z position.

A given ray tracing was repeated with successively smaller fixed increment $d\theta$ values until successive estimates of the final ray angle agreed to within 0.1°. Typically 100 to 600 steps were required, and 2° and 1° fixed increment values agreed to 0.1°.

Cusping of the ordinary ray was indicated by the phase angle approaching the magnetic field direction and the ray angle becoming perpendicular to it. When this condition was encountered to within $0.3d\theta$, the phase angle was stepped "across" the magnetic field, reversing the ray angle automatically by 180°, the ray tracing being continued in the customary manner. The region in which cusping occurred was limited, that is, if the ray were at some distance from the critical surface when it reached the magnetic field angle, cusping did not occur.

The axis for which an incident ray is scattered through an angle of 180° (overdense sphere) or 0° (underdense sphere) does not coincide with the axis of symmetry of the cloud because of the asymmetry introduced by the magnetic field. The displacement of the scattered ray was obtained from interpolation of the impact parameter values giving both positive and negative scattering.

Thus the output of the ray tracing program provides scatter angle versus impact parameter for ordinary and extraordinary rays for each field angle, frequency, and critical radius.

4. RESULTS AND DISCUSSION

In Figure 4, some typical ray paths are shown for zero field and for ordinary and extraordinary rays at a frequency of 3 MHz and a field angle of -45°. The ordinary and extraordinary rays show opposite asymmetries at a given field angle; for example, at $\theta_p = -45°$ the ordinary ray is displaced upward, whereas the extraordinary ray is displaced downward. At a field angle of 45° (not shown), the displacements are reversed, indicating a cyclic behavior. For an underdense sphere, the effect of a magnetic field is shown for the ordinary ray with $r_c = -0.50$ and $\theta_p = -45°$. The upward displacement of the rays is quite significant, leading to a large negative displacement for the ray scattered in the forward direction.

The variation of scattering cross section with scattering angle for zero field with critical radius as parameter is presented in Figure 5. The corresponding results for the magnetic field case are presented in Figures 6 through 9 for frequencies of 3 and 30 MHz and for field angles of 0°, ±45°, and 90°. The cross section has been expressed in terms of effective radius r_e corresponding to the radius of a

perfectly conducting sphere with the same cross section as the given sphere. Since there is little ray penetration into a highly overdense plasma (large r_c), and conversely, deep penetration into a slightly overdense or underdense plasma (r_c small or negative), it will be convenient to refer to these as "hard" and "soft" spheres, respectively.

For zero field, the cross section for hard spheres is high in the backscatter region, with very little change over a wide range of scattering angles. As the critical radius decreases, the backscatter cross section decreases rapidly along with a decrease in the range of substantially constant cross section. As we approach the critical density, $r_c = 1$, the cross section becomes negligible in the region from 90° to 180°. This result is indicated by a vertical line at $\theta = 90°$. For underdense spheres, the range of scattering angles is confined to the forward region, the cross section becoming large in the neighborhood of the maximum scattering angle. This effect, attributable to a small change in scattering angle with impact parameter in the region, has been indicated by a vertical line at maximum scattering. We note that the curves for different critical radii converge in the region of forward scatter, coalescence occurring at smaller angles as the critical radius increases. This behavior is derivable from the nature of forward scattering for which the impact parameter is large, with ray deflection occurring in the outer region where the electron density, together with its gradient, is small. Scattering, therefore, depends principally upon the impact parameter with little dependence upon the critical radius. The effect of critical radius, however, is not negligible when r_c is large (see Figure 2), resulting in the delayed convergence.

In general, the effect of a magnetic field is quite small at a frequency of 30 MHz, becoming appreciable at 3 MHz. The ordinary ray exhibits a minimum at a field angle of 90°; the minimum becomes more pronounced as the frequency is reduced from 30 to 3 MHz. A wavelike pattern is evident in several of the curves, particularly for the softer spheres at the lower frequency. It is difficult to find a simple explanation for this behavior because of the complexity of the computing process. However, a careful examination of the data indicates that the behavior is not spurious.

The curves for the extraordinary ray are quite smooth, bearing a closer resemblance to the zero field results than do those for the ordinary ray. At a frequency of 30 MHz, the results are very close to those for the zero field. However, the critically dense sphere now exhibits definite overdense characteristics, that is, a nonnegligible cross section in the backscatter region and a maximum scattering angle of 180°. As the frequency is decreased to 3 MHz the backscatter cross section rises substantially but the form of the curves remains unaltered. In addition, the range of overdense characteristics now extends to an underdense sphere with a

critical radius = -0.5. It thus appears that the principal effect of the field with respect to the extraordinary ray is that of increasing the effective critical radius of the cloud, giving it the characteristics of a hard sphere.

To show more pointedly the relation between cross section and scattering angle, polar diagrams are presented in Figures 10 through 12 for several field angles. To avoid negative values, the length of the radius vector has been taken as $1 + \log r_e$. Where the scattering is confined to the forward direction the maximum deflection angle has been indicated by a straight line from the origin. Because of the closeness of the curves in the forward direction, the corresponding values of r_c have been marked with respect to the maximum deflection lines.

As indicated previously, the calculation of the cross section requires the displacement δ from the axis of symmetry of the cloud, of the ray scattered through 180° or 0°. To show the characteristics of the displacement, we have plotted it as a function of field angle for several values of critical radius in Figure 13. Both the ordinary and extraordinary rays show a definite cyclic behavior with respect to θ_p. The magnitude of the displacement is a maximum near 45° and 135° and a minimum in the neighborhood of 0° and 90°. For the ordinary ray δ is negative for θ_p in the range 0°, 90° and positive in the range 90°, 180°, whereas for the extraordinary ray the sign is reversed. We may anticipate this behavior since, for example (Figure 4) the ordinary ray at $\theta_p = -45°$ range shows a downward bias near the axis of symmetry of the cloud, requiring a positive correction. The displacement is quite small for the extraordinary ray at both frequencies, but it shows a moderate increase for the ordinary ray when the frequency is decreased from 30 to 3 MHz. To show the behavior of the displacement over the entire range of critical radius, we have plotted δ as a function of r_c for a field angle of 45° (Figure 14). The displacement is a maximum at $r_c = 0$ for the ordinary ray, whereas for the extraordinary ray a maximum occurs at $r_c = -0.5$ at 3 MHz. For the extraordinary ray at 30 MHz and similarly for the other field angles (not shown), the displacements are too small for any great significance in the patterns.

To exhibit explicitly the effect of field angle upon the cross section, we have plotted r_e against θ_p with r_c as parameter (Figure 15). For reference the corresponding values for zero field are indicated in Figure 15a (ordinary ray). The ordinary ray shows a definite maximum at $\theta_p = 90°$ for both frequencies at backscatter. Further, to indicate the behavior at another scattering angle we have included the results for 90° scatter at 3 MHz. The pattern is quite different, with a minimum near $\theta_p = 45°$ and a maximum near 135°. The extraordinary ray shows a similar pattern except that a minimum is replaced by a maximum and vice versa, with variation not as great. In fact, at 30 MHz the $r_c = 0$ curve shows no dependence upon field angle.

The dependence of the maximum scattering angle for underdense spheres upon field angle and sphere hardness is shown in Figure 16 where θ_{max} is plotted as a function of θ_p for several values of r_c. The ordinary ray generally shows a weak dependence upon field angle except at 3 MHz and the higher values of r_c where the dependence can be considered as weak to moderate. For the extraordinary ray, there is virtually no dependence at 30 MHz and a rather weak variation at 3 MHz.

We have noted heretofore that the backscatter cross section for the extraordinary ray exhibits a strong similarity to that obtained for a hard sphere when no field is present, that is, high values of the cross section and a large range of backscatter angles over which the cross section is substantially constant. Furthermore, the dependence of the cross section upon field direction is rather weak. It is, therefore, natural to inquire whether the backscatter data for the extraordinary ray can be represented in terms of the critical radius for no field and the gyromagnetic ratio. Because of the small effect at a frequency of 30 MHz, we confine our analysis to 3 MHz, where $Y = 1/3$. Since the critical point for the extraordinary ray occurs at $X = 1 - Y$, a possible relation for a Gaussian distribution is

$$\begin{aligned} r_{ce}^2 &= r_c^2 - \ln(1-Y) \\ &= r_c^2 + 0.40 \text{ for } Y = 1/3, \end{aligned} \tag{9}$$

where r_{ce} is the effective critical radius which yields the same cross section at zero field as obtained with the given field. A plot of r_{ce}^2 against r_c^2 (Figure 17) shows that r_{ce}^2 is indeed a linear function of r_c^2 except at small values of r_{ce} where we do not expect the hard sphere concept to be accurate. The dependence of r_{ce} upon field angle shows up in the deviation in both intercept and slope of the straight line representing the data from the 45° line given by Eq. (9). The results for 45° and -45° are virtually the same and fairly close to the 45° line, with somewhat larger displacements for the 0° and 90° angles. Attempts to represent the angular dependence in terms of an effective average angle for the ray path have not proved fruitful. It is possible, however, to represent the data in a simple manner in terms of a modified form of Eq. (9), that is,

$$r_{ce}^2 = A[r_c^2 - \ln(1-Y)] + B, \tag{10}$$

where A and B are functions of θ_p. Evaluation of the A and B terms and using a parabola in sin θ_p to express field angle dependence yields

$$A = 1.055 - 0.090 \sin^2\theta_p$$

$$B = 0.15 - 0.23 \sin^2\theta_p . \qquad (11)$$

Although calculations at higher values of Y are not available, we may expect Eq. (10) to be a valid representation of the data. In fact, in view of the augmented hardness of the sphere at larger Y, the A and B coefficients should exhibit a weaker dependence upon field angle as Y increases. Since the effect of field angle is not large, it is useful to note the degree of error incurred in the cross section by use of the simplified Eq. (9) in place of the data. Although the deviation in r_{ce} is greatest at large values of r_c, the accuracy is best here because of the weak dependence of cross section upon critical radius when it is large. For example at $r_c = 1.41$ where log $r_e = 0.14$ at $\theta_p = 0°$, 0.12 at 45° and 0.08 at 90°, Eq. (9) yields 0.11; at $r_c = 0$, where log $r_e = -0.35$, at 0°, -0.42 at 45° and -0.51 at 90°, Eq. (9) yields -0.47. The cross section obtained from Eq. (9) may therefore be used as a reasonable average estimate when field direction effects are ignored.

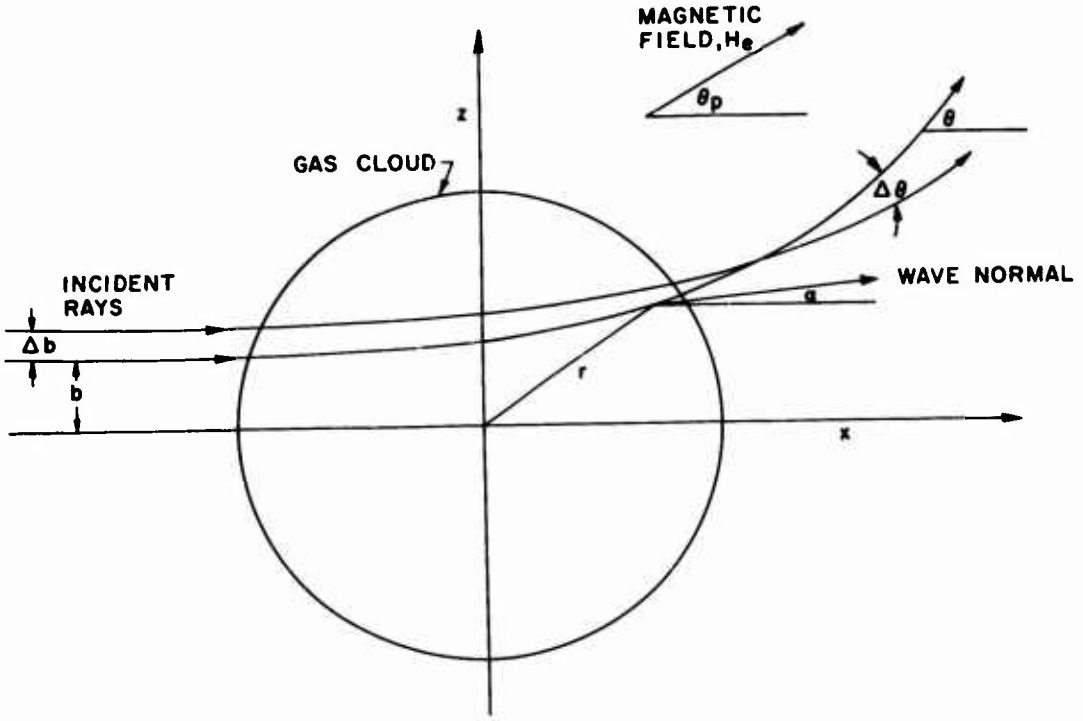

Figure 1. Geometry of Ray Path Through Gas Cloud in Presence of Magnetic Field

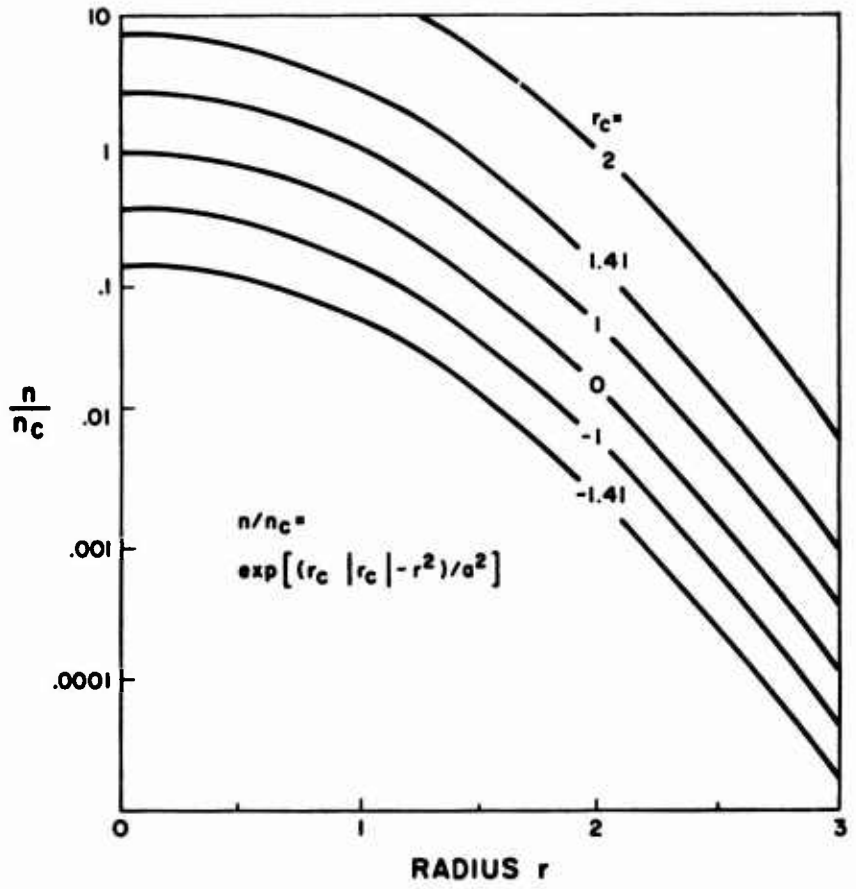

Figure 2. Electron Density Distribution of Gaussian Cloud for Several Values of r_c

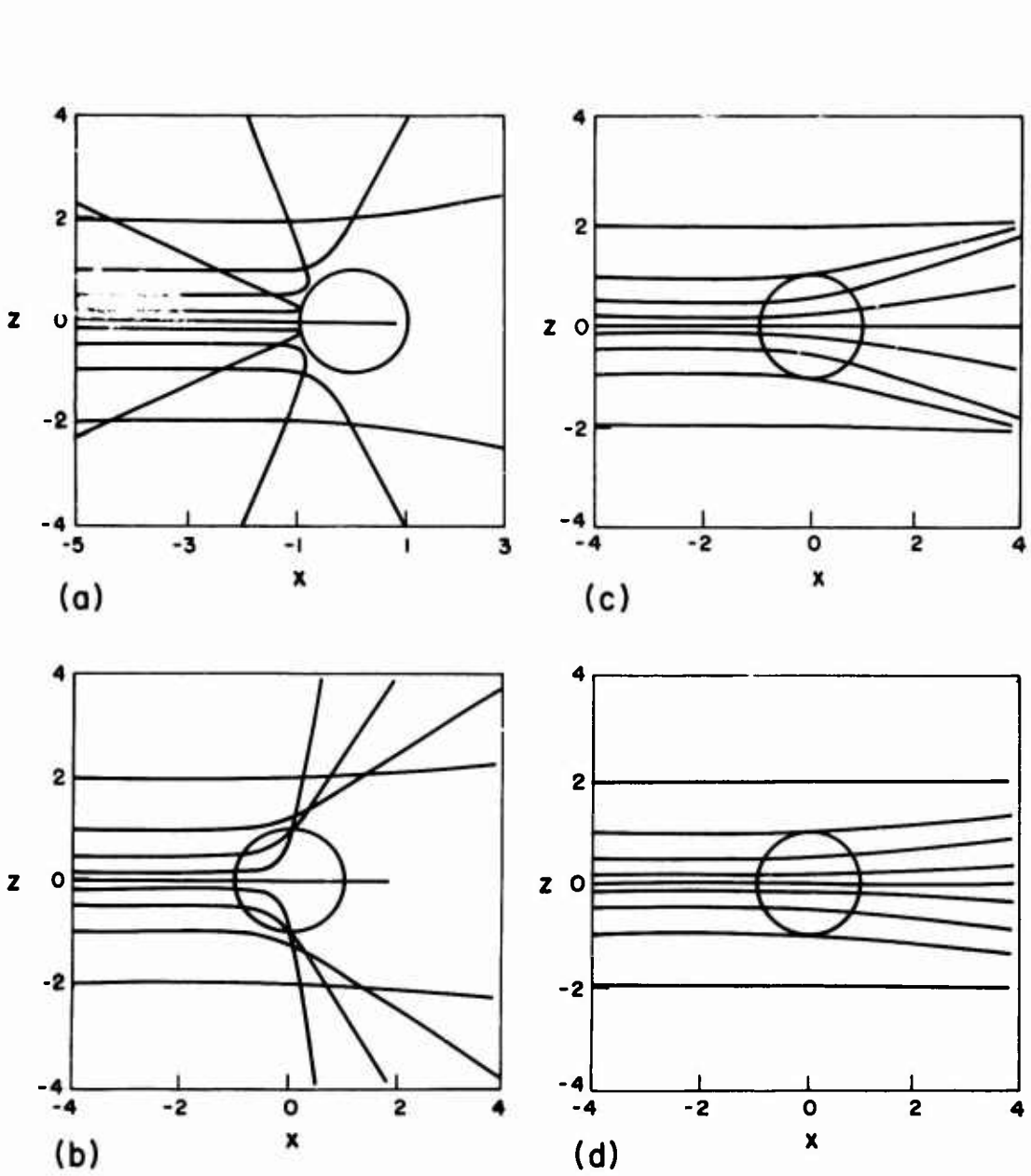

Figure 3. Ray Diagrams for Different Values of Critical Radius, 30 MHz Extraordinary Ray, $\theta_p = 0°$.

(a) $r_c = 1.0$; (b) $r_c = 0$; (c) $r_c = -1.0$; (d) $r_c = -1.41$

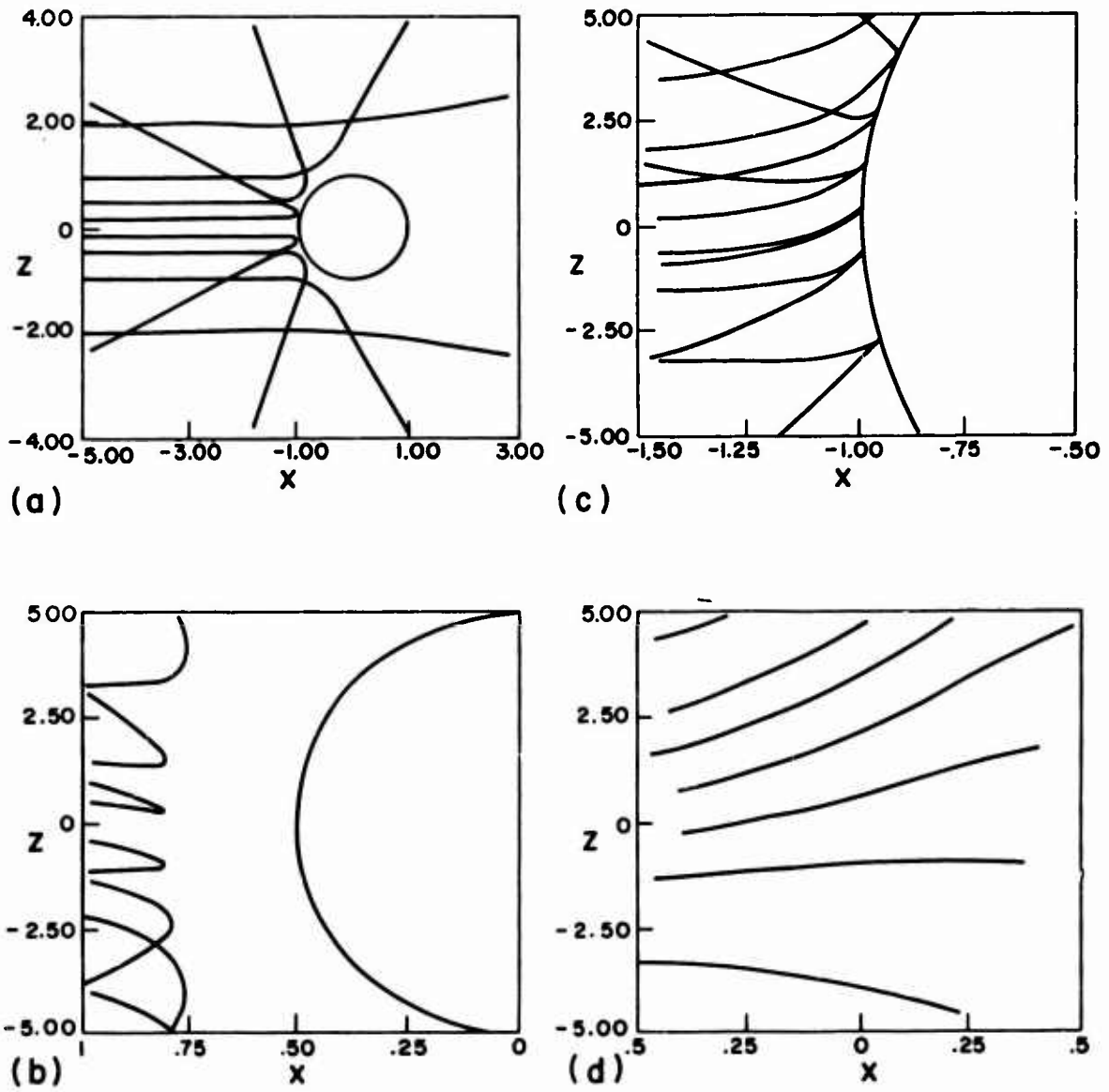

Figure 4. Typical Ray Paths Through Gas Cloud.
(a) $r_c = 1.0$, no field;
(b) $r_c = 0.5$, 3 MHz, extraordinary ray, $\theta_p = -45°$;
(c) $r_c = 1.0$, 3 MHz, ordinary ray, $\theta_p = -45°$;
(d) $r_c = -0.5$, 3 MHz, ordinary ray, $\theta_p = -45°$

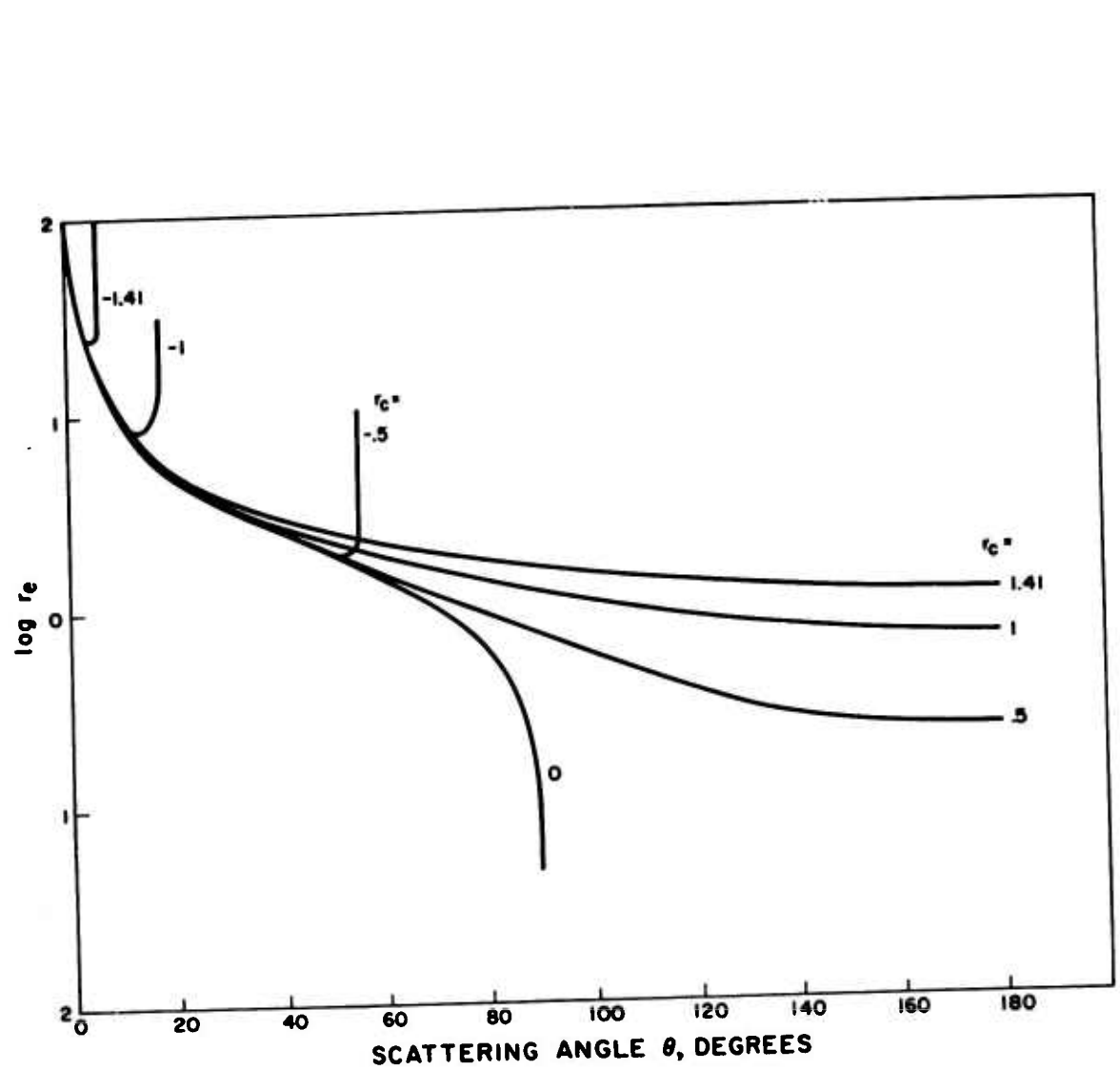

Figure 5. Variation of Effective Radius With Scattering Angle for Several Values of Critical Radius. No magnetic field

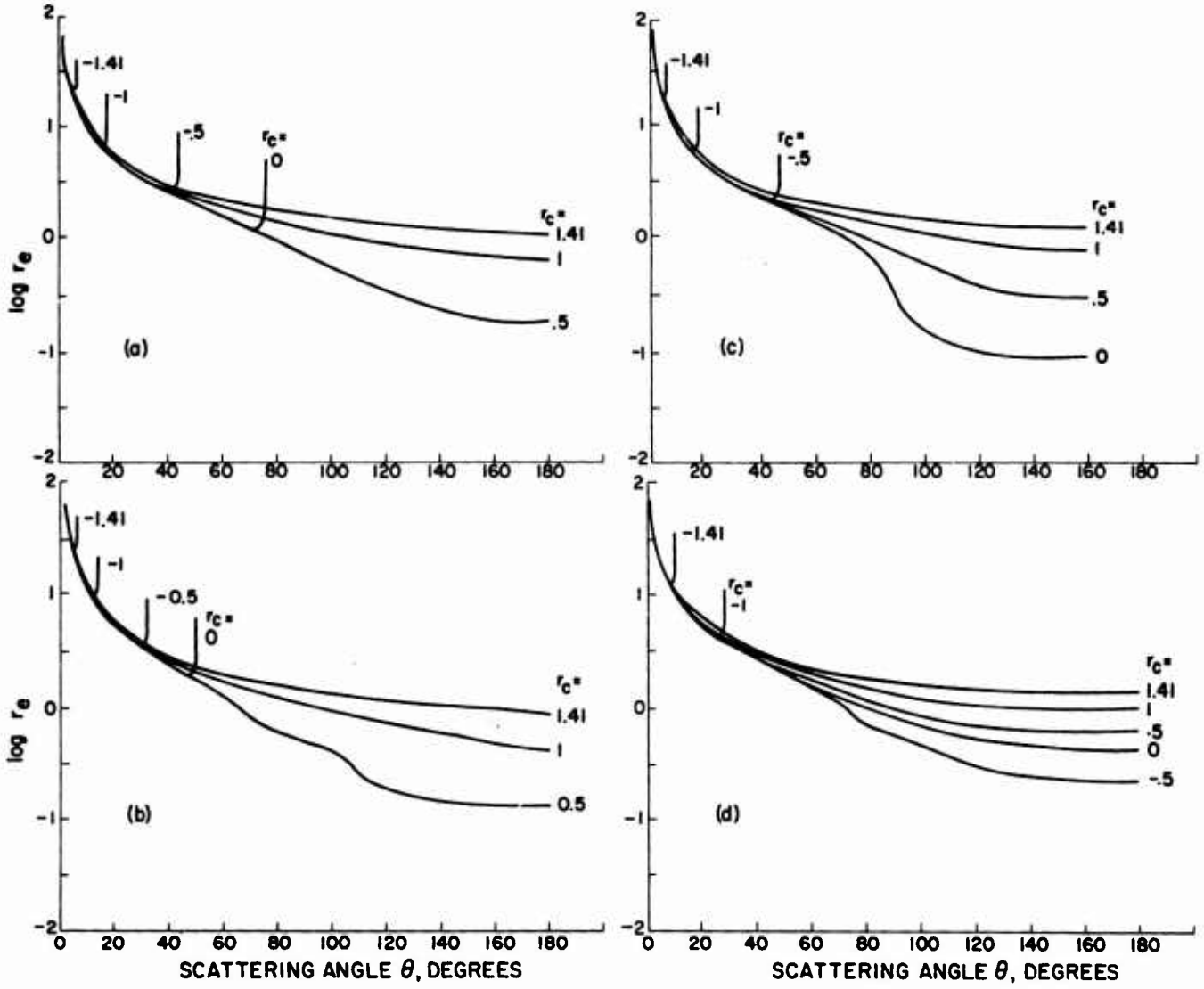

Figure 6. Variation of Effective Radius With Scattering Angle for Several Values of Critical Radius, $\theta_p = 0°$.
(a) ordinary ray, 30 MHz; (b) ordinary ray, 3 MHz; (c) extraordinary ray, 30 MHz; (d) extraordinary ray, 3 MHz

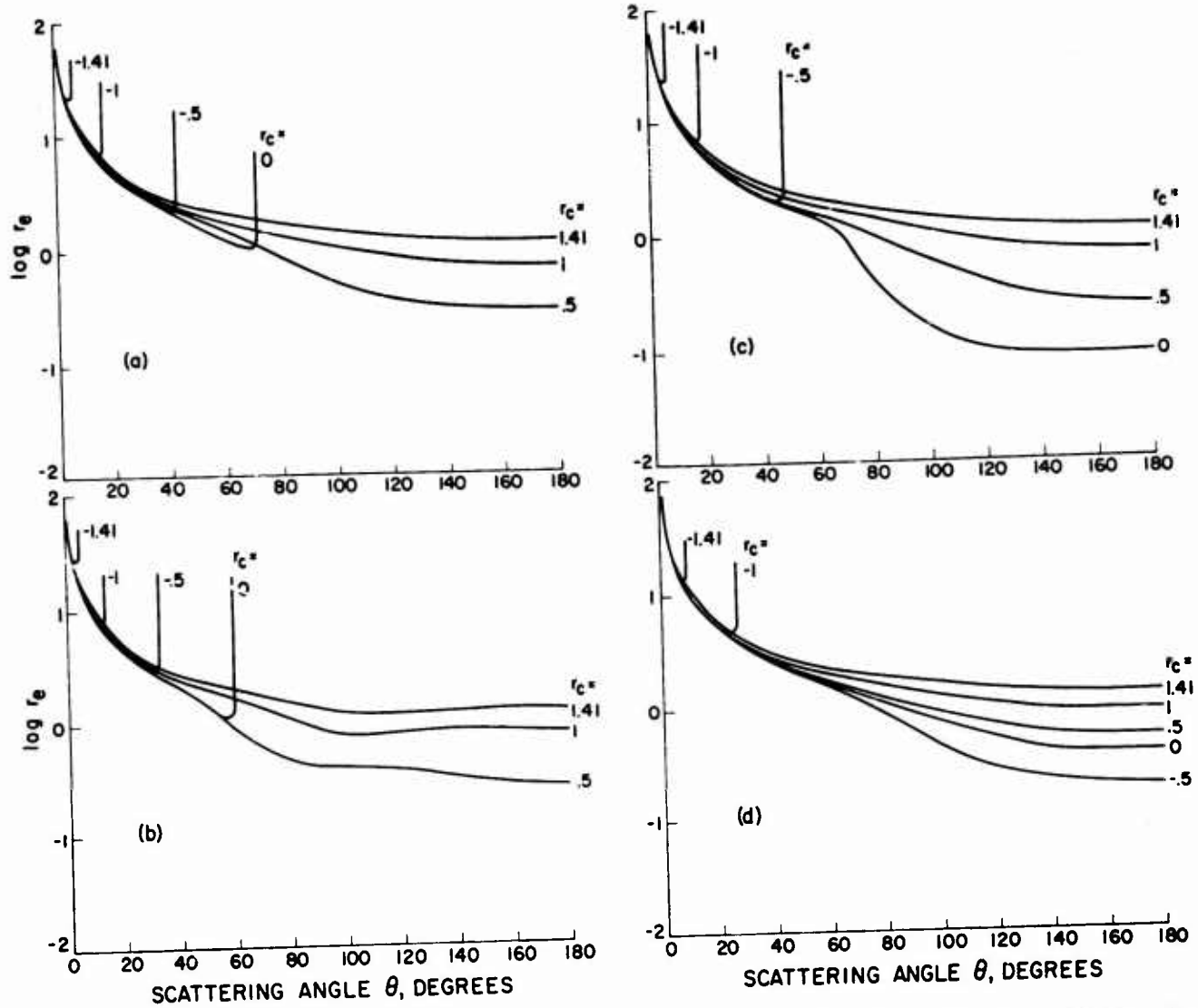

Figure 7. Variation of Effective Radius With Scattering Angle for Several Values of Critical Radius, $\theta_p = 45°$. (a) ordinary ray, 30 MHz; (b) ordinary ray, 3 MHz; (c) extraordinary ray, 30 MHz; (d) extraordinary ray, 3 MHz

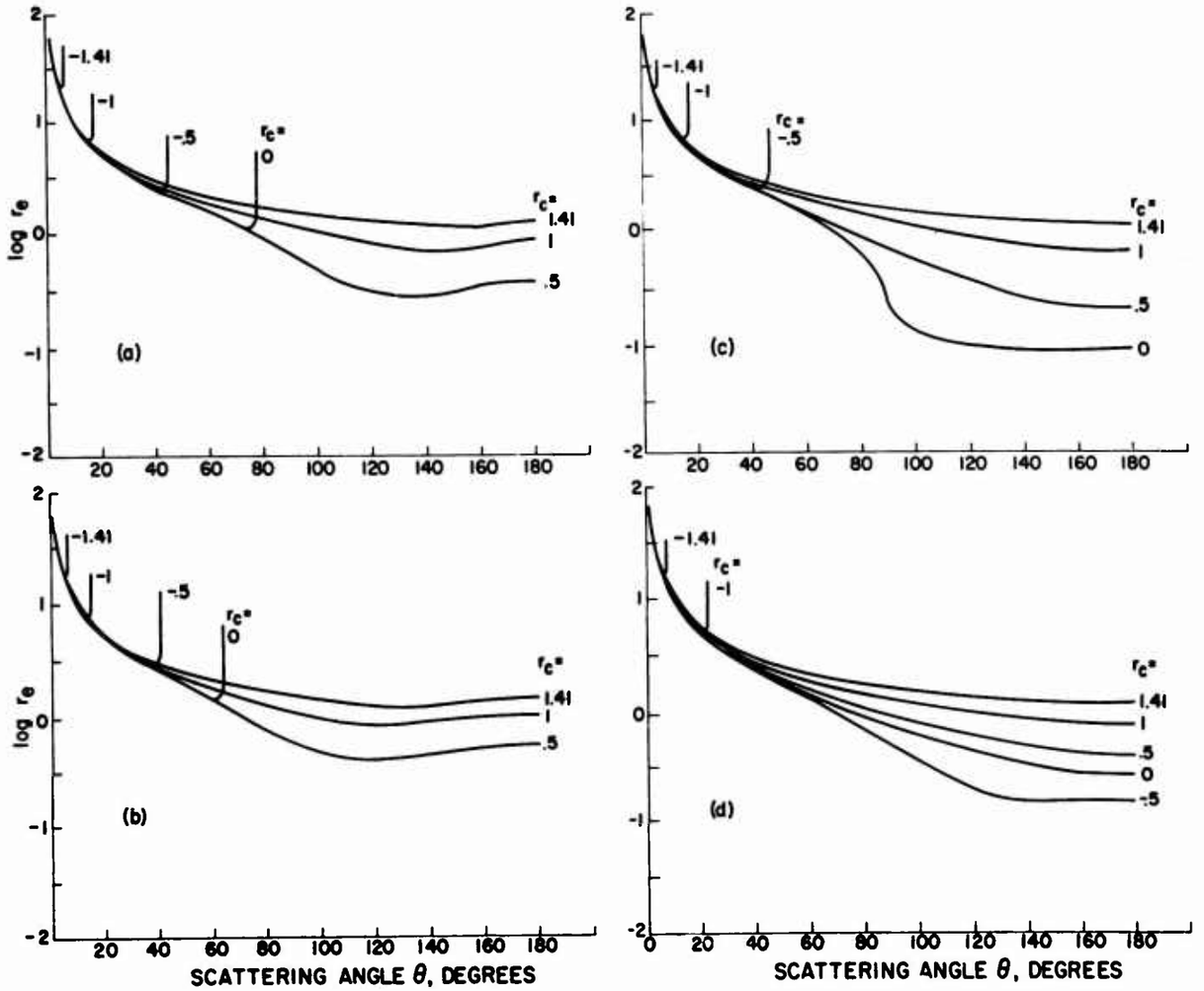

Figure 8. Variation of Effective Radius With Scattering Angle for Several Values of Critical Radius, $\theta_p = 90°$. (a) ordinary ray, 30 MHz; (b) ordinary ray, 3 MHz; (c) extraordinary ray, 30 MHz; (d) extraordinary ray, 3 MHz

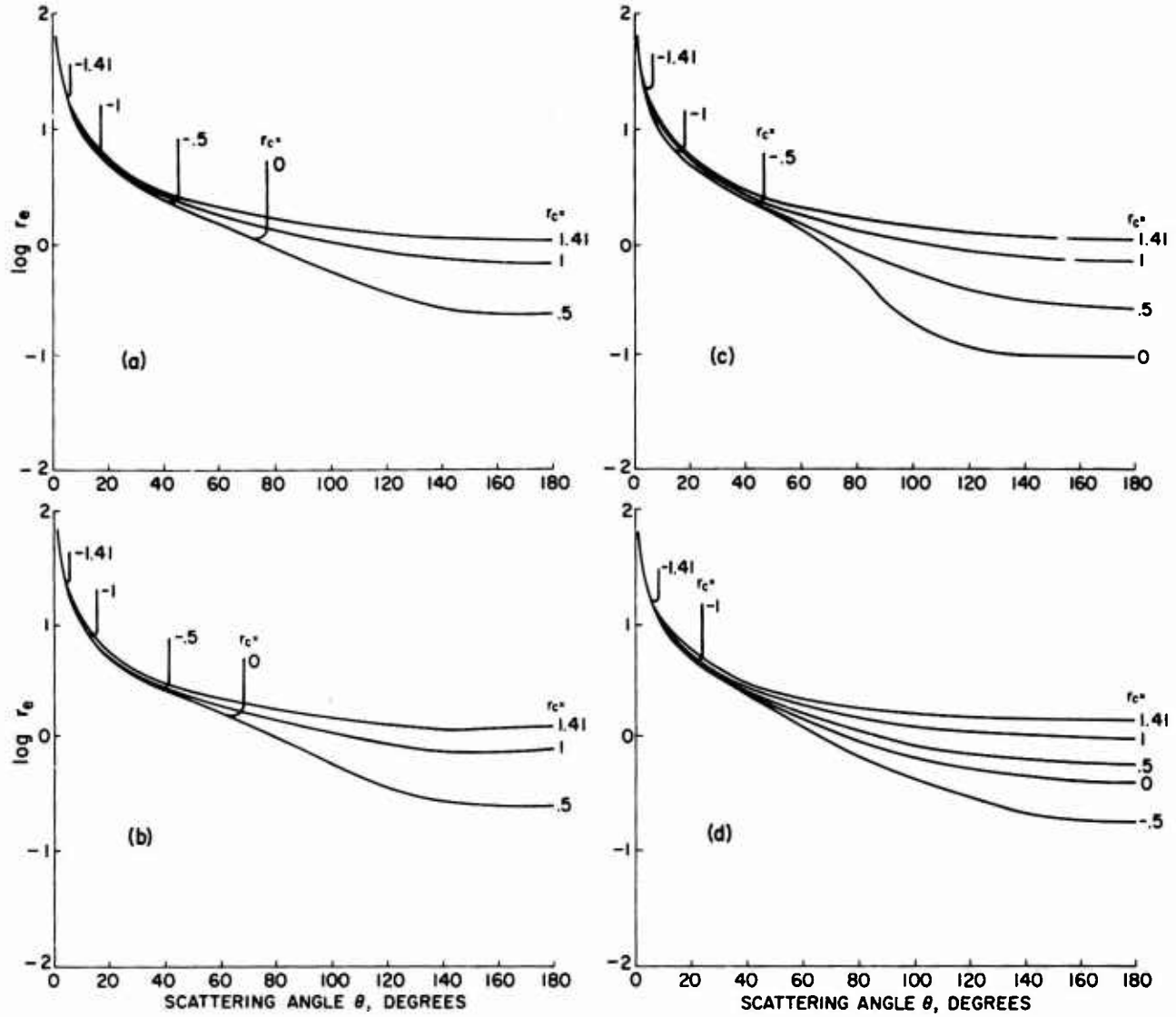

Figure 9. Variation of Effective Radius With Scattering Angle for Several Values of Critical Radius, θ_p = -45°. (a) ordinary ray, 30 MHz; (b) ordinary ray, 3 MHz; (c) extraordinary ray, 30 MHz; (d) extraordinary ray, 3 MHz

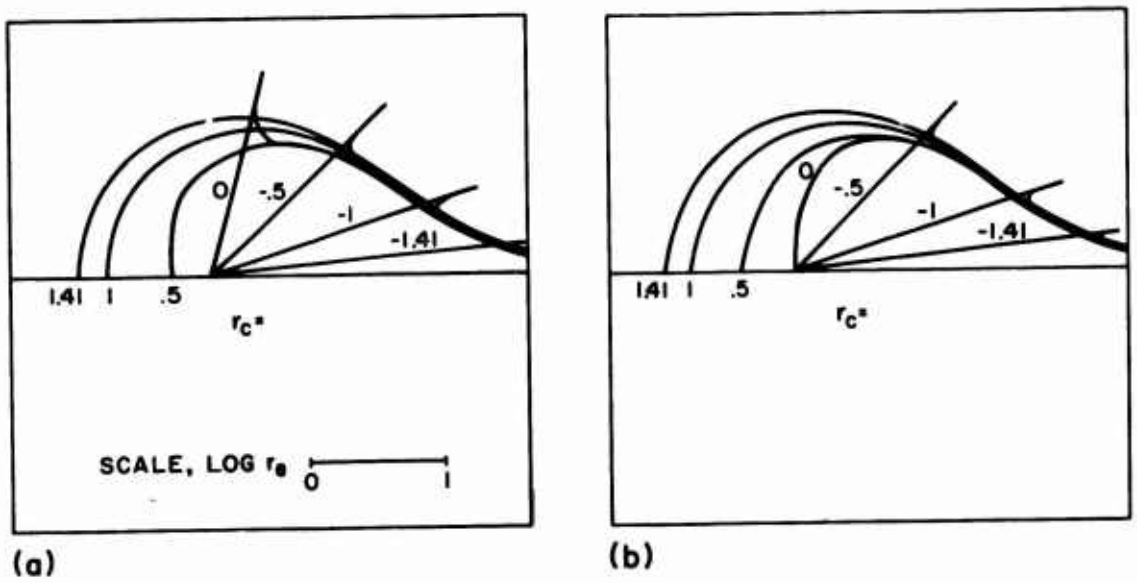

Figure 10. Polar Diagram of 1 + log r_e as a Function of Scattering Angle for $\theta_p = 0$.
(a) ordinary ray, 30 MHz; (b) extraordinary ray, 30 MHz

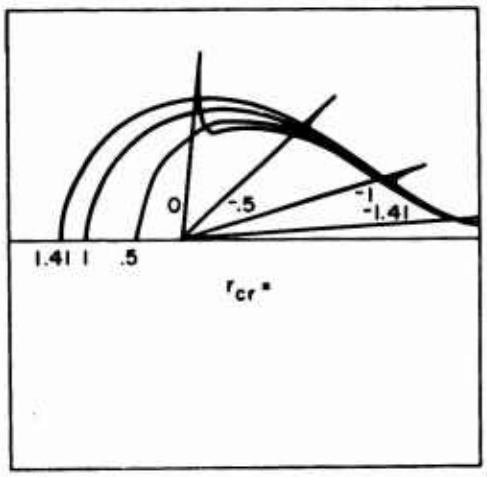

(a)

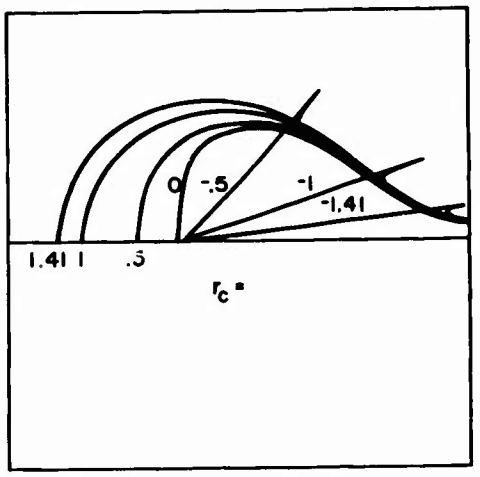

(c)

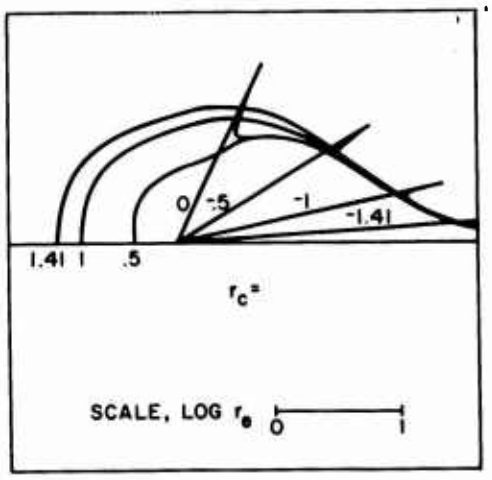

(b)

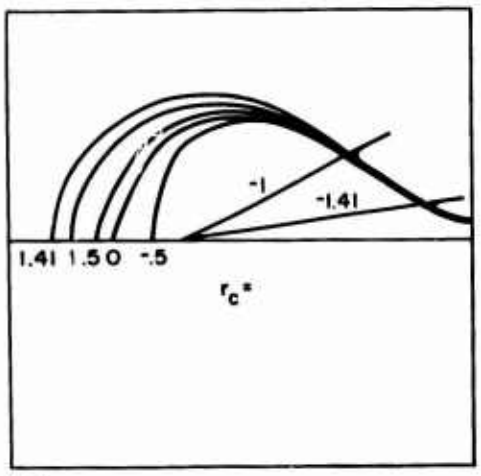

(d)

Figure 11. Polar Diagram of 1 + log r_e as a Function of Scattering Angle for $\theta_p = 45°$.

(a) ordinary ray, 30 MHz (b) ordinary ray, 3 MHz
(c) extraordinary ray, 30 MHz (d) extraordinary ray, 3 MHz

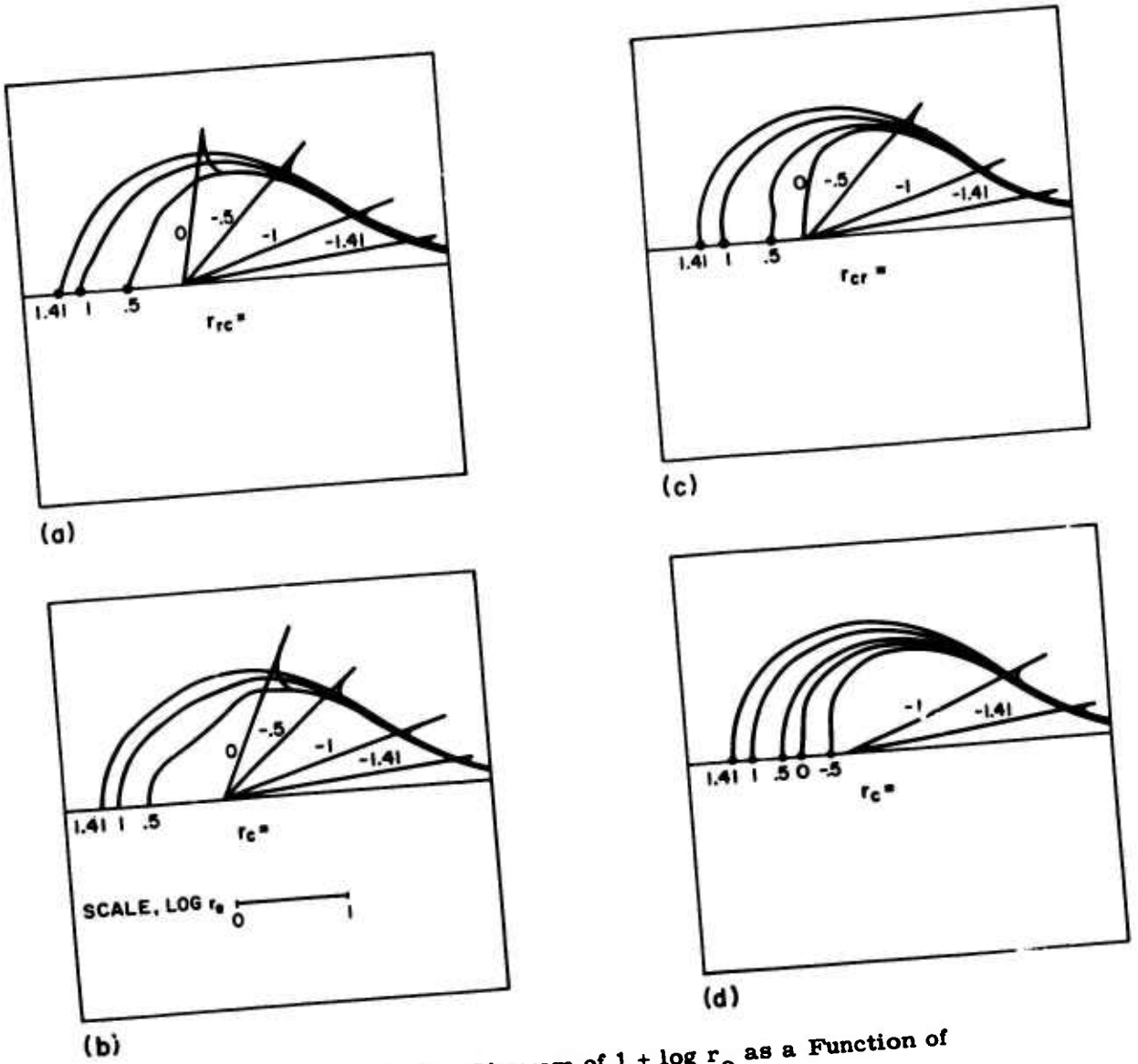

Figure 12. Polar Diagram of $1 + \log r_e$ as a Function of Scattering Angle for $\theta_p = 90°$.

(a) ordinary ray, 30 MHz (b) ordinary ray, 3 MHz
(c) extraordinary ray, 30 MHz (d) extraordinary ray, 3 MHz

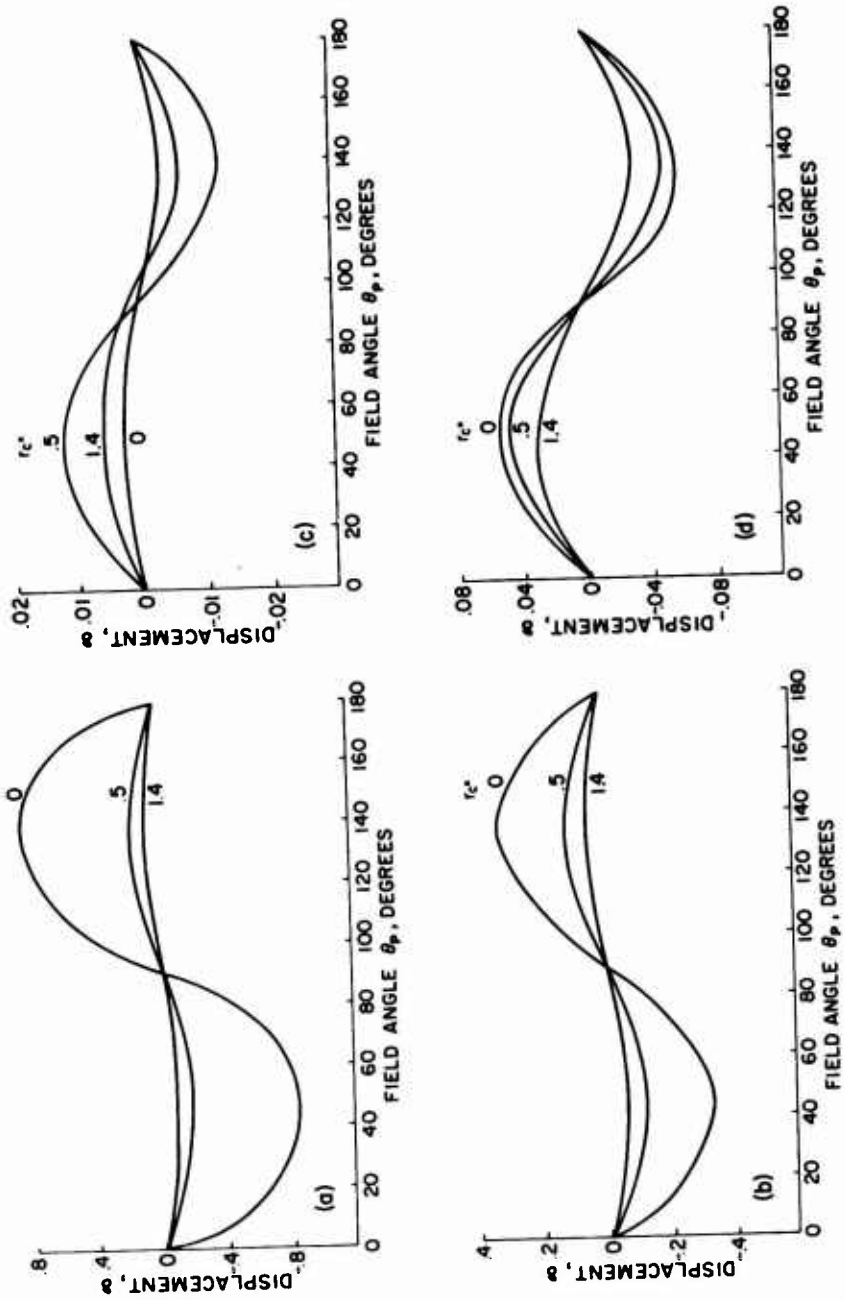

Figure 13. Displacement as a Function of Field Angle With Critical Radius as Parameter.
(a) ordinary ray, 30 MHz; (b) ordinary ray, 3 MHz; (c) extraordinary ray, 30 MHz; (d) extraordinary ray, 3 MHz

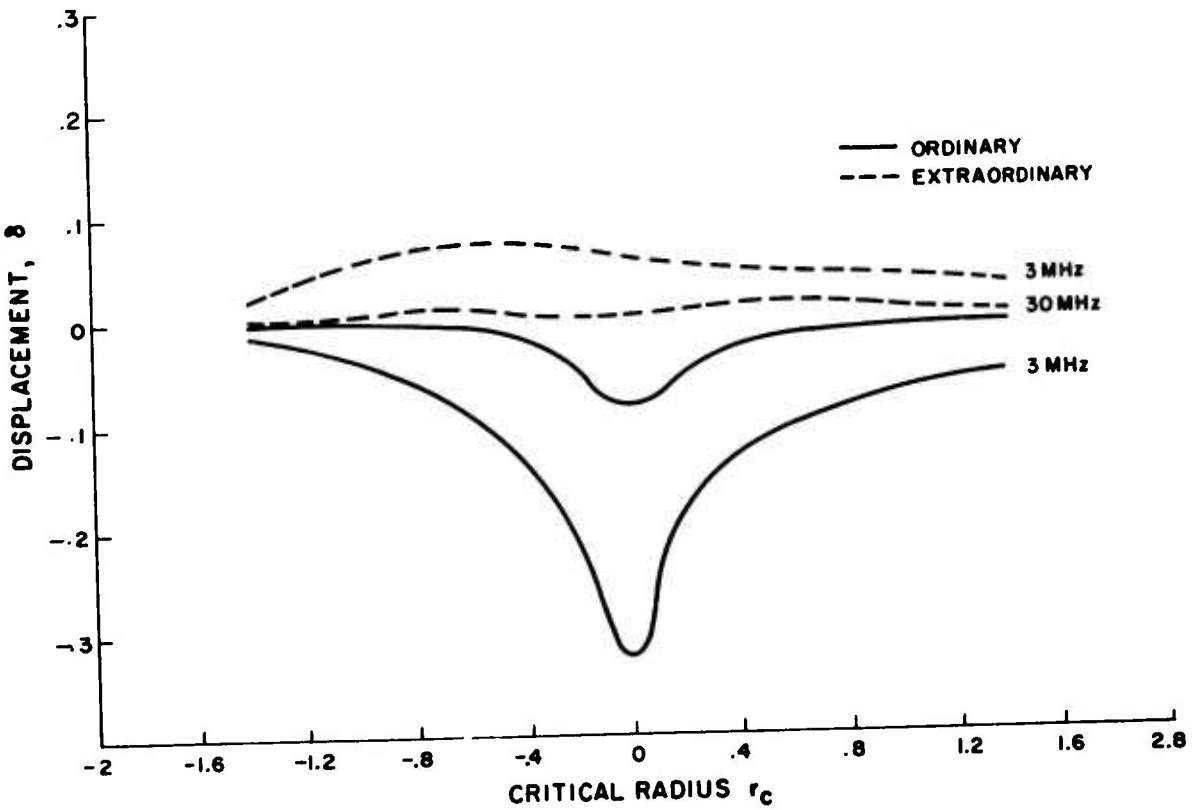

Figure 14. Displacement as a Function of Critical Radius With Frequency as Parameter; $\theta_p = 45°$

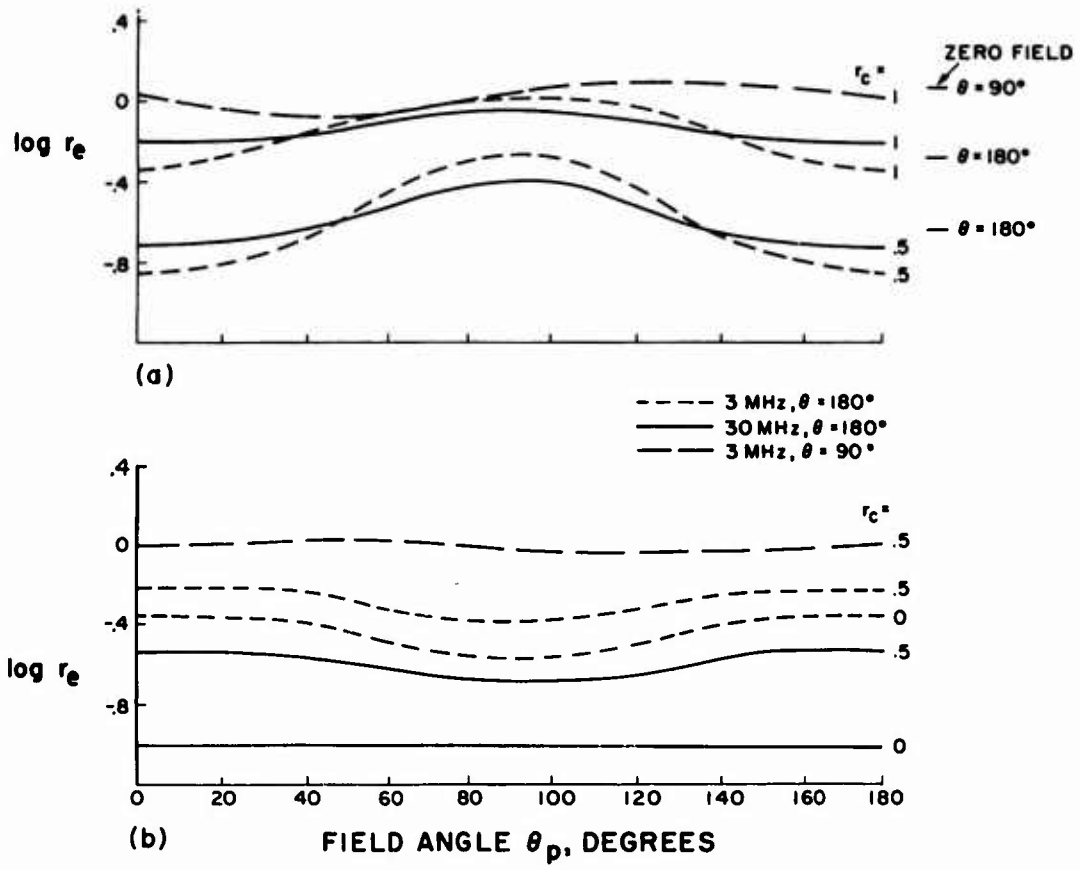

Figure 15. Cross Section as a Function of Field Angle With Critical Radius as Parameter for Scattering Angles of 90° and 180°.
(a) ordinary ray; (b) extraordinary ray

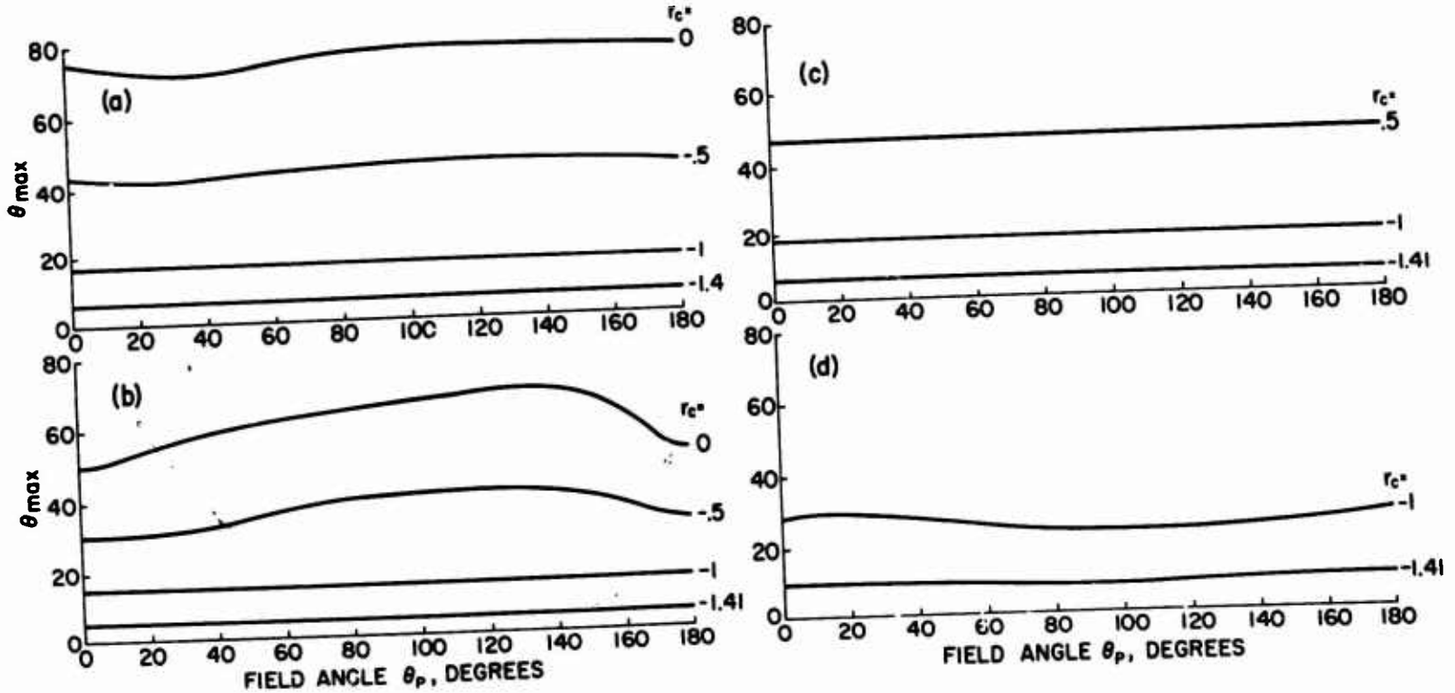

Figure 16. Maximum Scattering Angle for Underdense Spheres as a Function of Field Angle With Critical Radius as Parameter
(a) ordinary ray, 30 MHz; (b) ordinary ray, 3 MHz; (c) extraordinary ray, 30 MHz; (d) extraordinary ray, 3 MHz

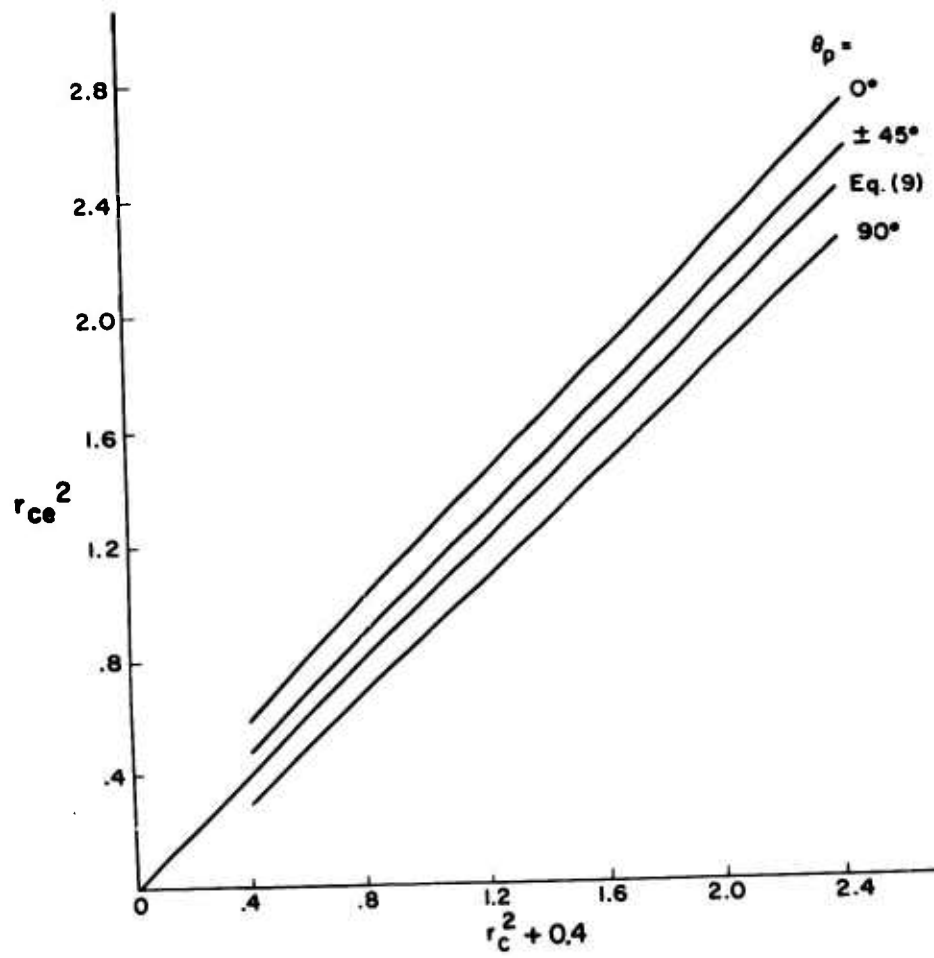

Figure 17. Plot of r_{ce}^2 Against r_c^2 With Field Angle as Parameter

References

Bohm, D. (1951) Quantum Theory, Prentice-Hall, New York, 522.

Budden, K.G. (1966) Radio Waves in the Ionosphere, Cambridge University Press, London, 250.

Haselgrove, J. (1955) Ray Theory and a New Method for Ray Tracing, Physical Society (London) Report of Conference of the Physics of the Ionosphere.

Kelso, J. (1964a) Radio Ray Propagation in the Ionosphere, McGraw-Hill, New York, 130.

Kelso, J. (1964b) Radio Ray Propagation in the Ionosphere, McGraw-Hill, New York, 328-331.

Klein, M.M. and Mabee, R.S. (1969) Scattering of HF Radio Waves by a Spherical Electron Cloud, AFCRL-69-0261.

Poeverlein, H. (1950) Strahlwege von Radiowellen in der Ionosphäre III, Z.angew. Phys., Vol. 2 (No. 4); 152-160.

Rosenberg, N.W., Klein, M.M., and Anderson, G. (1968) Microwave scattering from spherical electron clouds. In AGARD Conference Proceedings No. 37. Papers presented at the XIVth Symposium of the Electromagnetic Wave Propagation Committee of the Avionics Panel of AGARD, held at Sandefjord, Norway, 19th to 23rd August 1968.